

Non-Heme-Iron-Mediated Selective Halogenation of Unactivated Carbon–Hydrogen Bonds

Katharina Bleher,^[a] Peter Comba,^{*[a]} Dieter Faltermeier,^{+, [a]} Ashutosh Gupta,^[a] Marion Kerscher,^[a] Saskia Krieg,^{+, [a]} Bodo Martin,^[a] Gunasekaran Velmurugan,^[a] and Shuyi Yang^[a]

Abstract: Oxidation of the iron(II) precursor $[(L^1)Fe^{II}Cl_2]$, where L^1 is a tetradentate bispidine, with soluble iodosylbenzene (⁵PhIO) leads to the extremely reactive ferryl oxidant $[(L^1)(Cl)Fe^{IV}=O]^+$ with a *cis* disposition of the chlorido and oxido coligands, as observed in non-heme halogenase enzymes. Experimental data indicate that, with cyclohexane as substrate, there is selective formation of chlorocyclohexane, the halogenation being initiated by C–H abstraction and the result of a rebound of the ensuing radical to an iron-bound Cl^- . The time-resolved formation of the halogenation product indicates that this primarily results from ⁵PhIO oxidation of an initially formed oxido-bridged diiron(III)

resting state. The high yield of up to >70% (stoichiometric reaction) as well as the differing reactivities of free Fe^{2+} and Fe^{3+} in comparison with $[(L^1)Fe^{II}Cl_2]$ indicate a high complex stability of the bispidine-iron complexes. DFT analysis shows that, due to a large driving force and small triplet-quintet gap, $[(L^1)(Cl)Fe^{IV}=O]^+$ is the most reactive small-molecule halogenase model, that the Fe^{III} /radical rebound intermediate has a relatively long lifetime (as supported by experimentally observed cage escape), and that this intermediate has, as observed experimentally, a lower energy barrier to the halogenation than the hydroxylation product; this is shown to primarily be due to steric effects.

Introduction

Due to its importance for biological systems and in industrial processes for polymer and bulk chemical production as well as for bioactive and medicinal products, the challenging selective functionalization of inert C–H bonds is of fundamental interest and of great importance.^[1–7] In industry a large fraction of these transformations is carried out with harmful oxidants and under harsh conditions. The halogenation of hydrocarbon substrates is of particular interest, and nature uses either the heme-dependent haloperoxidases or, with dioxygen as oxidant, flavin-dependent or non-heme-iron halogenases.^[8] While chloroperoxidases exploit heme-iron-bound hypochlorite to halogenate electron-rich substrates, non-heme halogenases have an iron(IV)-oxido active center that is even able to abstract a hydrogen atom from electron-poor alkanes in the rate

determining step and then produces the halogenated product in a rebound reaction.^[9] The α -ketoglutarate-dependent non-heme-iron halogenases, for example SyrB2, have active sites similar to those of oxidases such as Tau-D but instead of hydroxylating alkanes selectively halogenate unactivated organic substrates.^[8,9] In enzymes, the selectivity of halogenation versus hydroxylation is partially due to the positioning by the protein of the substrate radical produced in the first step of the reaction.^[10–12] Various small-molecule non-heme-iron complexes have been established as mechanistic models for non-heme-iron halogenases and/or have been shown to be able to halogenate alkanes in presence of oxidants such as H_2O_2 or oxygen atom transfer agents [e.g., iodosylbenzene (PhIO) or meta-chloroperoxybenzoic acid (mCPBA)].^[13–18] There are few examples, where the natural oxidant dioxygen is used to produce high-valent oxido complexes,^[19–21] and examples of halogenase mimics that operate by mechanisms different from that observed in the enzymes have also been described.^[22]

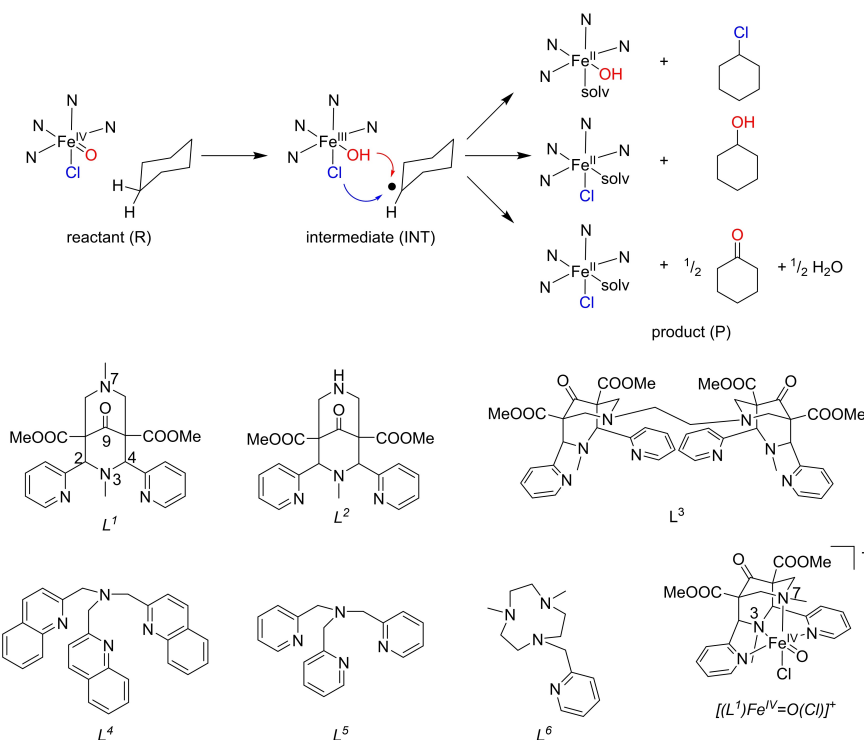
In bioinspired model systems supposed to mimic the enzyme mechanism, that is, starting with C–H abstraction by an iron(IV)-oxido species with a *cis*-disposed chloride, followed by a rebound step of the organic substrate radical to the hydroxido-chlorido-iron(III) intermediate (Scheme 1), the selectivity for halogenation over hydroxylation covers the full range from 100% hydroxylation to selective halogenation (Table 1). Here, we discuss the only system featuring selective halogenation on the basis of a recent thorough mechanistic study^[23] and further experimental and computational data, and also consider other small-molecule non-heme-iron halogenase model systems with differing electronic and steric properties of the

[a] Dr. K. Bleher, Prof. Dr. P. Comba, Dr. D. Faltermeier,⁺ Dr. A. Gupta, Dr. M. Kerscher, Dr. S. Krieg,⁺ Dr. B. Martin, Dr. G. Velmurugan, S. Yang
Universität Heidelberg
Anorganisch-Chemisches Institut und Interdisziplinäres Zentrum für Wissenschaftliches Rechnen (IWR), INF 270
69120 Heidelberg (Germany)
E-mail: peter.comba@aci.uni-heidelberg.de

[†] The results described are part of the PhD theses of Dieter Faltermeier and Saskia Krieg.

Supporting information for this article is available on the WWW under <https://doi.org/10.1002/chem.202103452>

© 2021 The Authors. Chemistry - A European Journal published by Wiley-VCH GmbH. This is an open access article under the terms of the Creative Commons Attribution Non-Commercial NoDerivs License, which permits use and distribution in any medium, provided the original work is properly cited, the use is non-commercial and no modifications or adaptations are made.



Scheme 1. The non-heme-iron halogenase mechanism, ligands discussed and structure of the bispidine-iron(IV)-oxido-chlorido complex with the tetradentate bispidine L^1 .

Table 1. Reported halogenation versus hydroxylation selectivities of the non-heme-iron model systems $[(L^n)(Cl)Fe^IV=O]^+$ ($n = 1, 4, 5, 6$).

| Ligand | Formation of $[(L^n)(Cl)Fe^IV=O]^+$ | % R-Cl | % R-OH | % R=O | Ref. |
|--------|-------------------------------------|--------|------------------|------------------|---------|
| L^1 | oxidation, 3PhIO | 100 | 0 | 0 | [23] |
| L^4 | ligand exchange ^[a] | 78 | 15 | 7 | [16] |
| L^5 | ^[a] or oxidation, TBHP | 85 | 0 | 15 | [13,16] |
| L^6 | ligand exchange ^[a] | 0 | — ^[b] | — ^[b] | [15] |

[a] Produced by exchange of MeCN with Cl^- at the $[(L^n)(MeCN)Fe^IV=O]^{2+}$ precursor. [b] Not reported.

ferryl oxidant and divergent halogenation/hydroxylation ratios.^[13–16]

Results and Discussion

Preamble

Iron-(IV) oxido complexes of the tetradentate bispidine ligand L^1 , with acetonitrile (MeCN), Cl^- or Br^- as monodentate coligand, have the oxido group *trans* to N3 and therefore the coligand coordinated in the *xy*-plane (Scheme 1), where the latter influences the in-plane ligand field, specifically the energy of the $d_{x^2-y^2}$ orbital.^[23] This can be monitored by optical spectroscopy, where the corresponding d–d transition is low in energy (for the L^1 -based ferryl complex shifting from 768 to 850 and 900 nm for the complexes with MeCN, Cl^- and Br^- *trans* to N7,

respectively) but still indicates an intermediate-spin ($S=1$) ground state albeit with decreasing triplet–quintet gap.^[23,24] C–H abstraction by high-valent non-heme-iron oxidants generally proceeds on the quintet surface, with a preference for the σ channel with a linear $[Fe-O\cdots H\cdots C-R]$ transition state and transfer of the electron into the d_{z^2} orbital. All non-heme-iron enzymes have in contrast to many intermediate-spin ($S=1$) model systems a high-spin ($S=2$) ground state.^[25–28] Therefore, the L^1 based ferryl complex discussed here has “the wrong spin ground state” but is the most reactive low molecular weight non-heme-iron model system, as fast as some enzymes and much faster than the L^4 based complex with a quintet ground state (see the Supporting Information for a comparison of relevant kinetic parameters).^[23] A plausible reason for the unprecedented reactivity of this $S=1$ $Fe^IV=O$ species is the rigid and for $Fe^IV=O$ slightly too large bispidine cavity that provides four nitrogen donors and enforces a short Fe^IV-N3 bond (*z*-axis) and a longer and more flexible Fe^IV-N7 bond (*xy*-plane).^[29–31] The large cavity leads to one of the thermodynamically strongest ferryl oxidants,^[32–35] and the relatively long Fe^IV-N7 distance together with the possibility to select a weak monodentate ligand *trans* to N7 yields a small in-plane ligand field and therefore a small triplet–quintet gap. This is supported by the observation that the reactivities strongly depend on the monodentate coligand in the predicted order ($MeCN < Cl^- < Br^-$).^[23] The in-plane ligand field may be further tuned by the substituent at N7 (L^1 vs. L^2)^[23,36] and substituents at the pyridine groups.^[34,38]

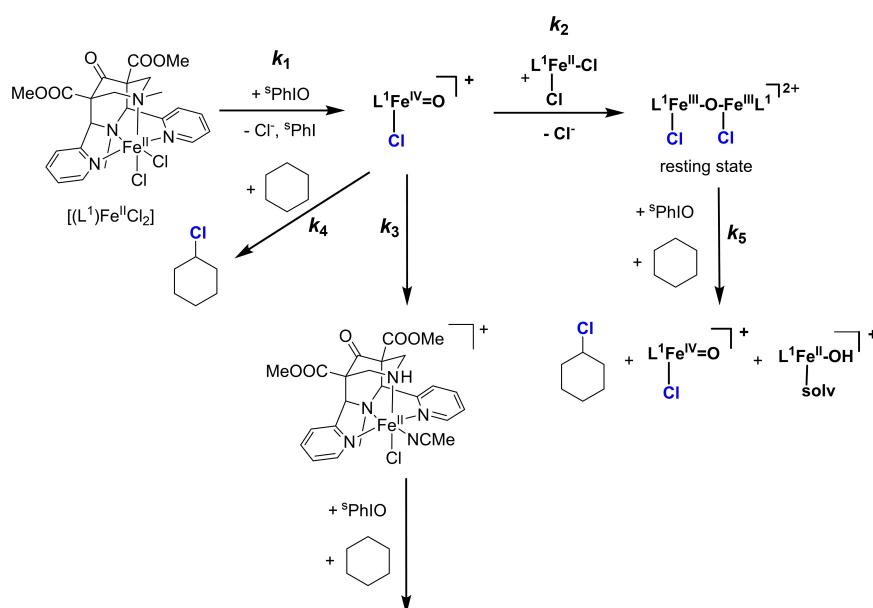
The proposed mechanism for the halogenation of cyclohexane by $[(L^n)(Cl)Fe^{IV}=O]^+$ ($n = 1, 2$) is shown in Scheme 1 (data from the published kinetic analysis are given in the Supporting Information). The initial step is C–H abstraction by the ferryl oxidant, and for the L^1 -based system, this is inferred from second-order kinetics with the substrate^[23] and experimentally determined kinetic isotope effects and product distributions with adamantane as substrate.^[14,39,40] The rebound step at the iron(III)/radical intermediate is supported by the observation that addition of external Cl^- decreases the yield of halogenated product (see below) because free Cl^- is oxidized to ClO^- . This consumes the ferryl species, and the hypochlorite is not able to transform the substrate to the halogenated product (see the Supporting Information for a more detailed discussion of the Cl^- oxidation [ClO^- formation] experiments).^[23] Importantly, from the fact that Cl^- is not stable in presence of $[(L^1)(Cl)Fe^{IV}=O]^+$, it follows that the chlorine atom in the product must emerge from an iron-bound Cl^- , that is, according to a rebound pathway.

An interesting observation was that, while the half-life of the ferryl complex in presence of the cyclohexane substrate at $-90^\circ C$ is only of the order of seconds, the halogenation of cyclohexane in bulk reactions with excess iodossylbenzene as oxidant takes hours at ambient temperature (see below). This apparent ambiguity might derive from two factors: i) The ferryl complex decays in three parallel reactions (Scheme 2). From the kinetic analysis it follows that the halogenation (pathway with k_4) competes with inner-sphere C–H activation – demethylation at the tertiary amine N7 (a first-order process with k_3 that, depending on the conditions, is 1–2 orders of magnitude slower than the reaction with substrate and can be excluded with L^2) – and with the second-order comproportionation of the iron(IV) product with unreacted iron(II) precursor, producing the very stable diiron(III) “resting state” (a second-order process with k_2

that depends on the formation rate of the ferryl complex and, depending on the conditions can be of similar efficiency as the halogenation pathway).^[23] ii) Part of the cyclohexyl radical intermediate (pathway with k_4) might decay unproductively, that is, by cage escape. Pathways other than rebound, that is, combination of the organic radical either with the $Fe^{III}-OH$ or the $Fe^{III}-Cl$ site at the intermediate (Scheme 1), generally called cage escape, become important with increasing life-time of the intermediate and this was probed experimentally for the bulk reaction (see the Supporting Information for details).^[23] From the kinetic parameters (see Table S1 in the Supporting Information),^[23] it follows that at low temperature, the pathways with k_2 (comproportionation) and k_4 (halogenation) occur in a ratio of around 1:2 with only traces of demethylation (k_3) predicted to be observed. However, differing temperature dependences of the rate of all four reactions involved may lead to a situation, where in the bulk reaction significantly less than 10% halogenation and primarily comproportionation result. According to the experimental data (see Figure 1 below), most of the halogenation product of bulk reactions results from oxidation of the diiron(III) resting state (pathway with k_5), and this is a very slow process. This mechanistic scenario (Scheme 2) is consistent with all currently available experimental data and therefore is the basis for the interpretation of the data presented here.^[41]

Analysis of the experimental data

Halogenation reactions were carried out with 5PhIO ($^5PhIO = 1-(tert\text{-butylsulfonyl})-2\text{-iodossylbenzene}$) in MeCN, and the product yields were determined by gas chromatography (GC, see Experimental Section and Supporting Information). An important consequence of the extraordinary reactivity of



Scheme 2. Proposed mechanism of oxidation with high-valent iron–bispidine complexes.

$[(L^1)(Cl)Fe^{IV}=O]^+$ is the fast comproportionation (pathway with k_2 in Scheme 2), which can only be suppressed by increasing the formation rate of $[(L^1)(Cl)Fe^{IV}=O]^+$ (low concentration of the Fe^{II} precursor), and this requires a large excess of the external oxidant. The consequence is that in mechanistic work with these systems stoichiometric reactions are largely excluded (Table 2). 5PhIO has a higher solubility than $PhIO$ and, therefore, with $[(L^1)(Cl)Fe^{IV}=O]^+$ a slightly higher yield of the chlorocyclohexane product than published before was expected and is observed (47.0 vs. 39.9%) but with the same product selectivity (>99.5% halogenation, see the Supporting Information for yields of various side products).^[14] Reaction times shorter than 24 h lead to a significantly lower yield of the chlorocyclohexane product (see time-dependent measurements, blue squares in Figure 1). Kinetic and thermodynamic parameters generally need to be determined under controlled and constant conditions, for example, constant ionic strength. Some of our measurements (kinetics and product yields) were therefore performed with added electrolyte (NBu_4PF_6 or NBu_4Cl , see Table 2). While added NBu_4PF_6 does not lead to any significant change of product ratios (i.e., the ionic strength does not significantly influence the yield in the range tested here), addition of NBu_4Cl drastically reduces the formation of chlorocyclohexane. We have shown that this is due to the oxidation

of Cl^- to ClO^- ,^[23] where the latter is not able to oxidize cyclohexane. The important mechanistic consequence is that iron-bound rather than free Cl^- is required for the substrate halogenation, that is, this occurs via a rebound process as indicated in Scheme 1 (see the Supporting Information for a detailed discussion of the oxidation reaction of Cl^- to ClO^-). Unfortunately, this obviously excludes catalytic halogenation, where external Cl^- needs to exchange with a solvent molecule at the Fe^{II} precatalyst to complete the catalytic cycle. However, as discussed above, the reactions described here in general had to be performed in an excess of terminal oxidant (5PhIO , generally 10 equiv.), that is, under catalytic reaction conditions with respect to the C–H activation step (see also the three entries in Table 2 with stoichiometric amounts of oxidant, thus indicating that stoichiometric reactions largely produce the comproportionation product; this is also supported by ESI-MS analyses^[23]).

One of the side reactions that leads to an unproductive decay of the active $[(L^1)(Cl)Fe^{IV}=O]^+$ species is demethylation at N7 (pathway with k_3 in Scheme 2), and this may be prevented by using the demethylated ligand to produce the ferryl oxidant, that is, the L^2 based Fe^{II} precursor. It has been shown that with 5PhIO this forms an active ferryl complex, $[(L^2)(Cl)Fe^{IV}=O]^+$ with a triplet ground state but, due to small changes in the ligand field (secondary vs. tertiary amine at N7) with a larger triplet-quintet gap ($d_{x^2-y^2}$ transition at 815 vs. 850 nm) and a slightly smaller reactivity.^[23,42] However, the observed yield of chlorocyclohexane in the bulk reaction (selective halogenation as with the L^1 -based system) is significantly higher with the demethylated precursor (74 vs. 47%; Table 2), and this might at least partially be due to the suppression of one of the side reactions but the small changes in the electronic structure of the oxidant may also play a role. Moreover, the less sterically demanding site might also be beneficial for the structural changes necessary in the rebound process.

The other side reaction that has been studied in detail before is the formation of the oxido-bridged diiron(III) complex $\{[(L^n)(Cl)Fe^{III}]_2O\}^{2+}$ ($n=1, 2$), a type of species that generally is considered to be rather unreactive.^[23] Due to a relatively fast formation rate of the dinuclear complex, after a fast initial phase the latter is the major species in solution and therefore proposed to be responsible for the observed formation of chlorocyclohexane in the bulk reactions.^[23] An important observation is that, with stoichiometric amounts of 5PhIO as the terminal oxidant, there is only a negligible amount of halogenation product (Table 2). This supports our mechanistic proposal, indicating that the reaction of the “resting state” (the oxido-bridged diiron(III) complex $\{[(L^n)(Cl)Fe^{III}]_2O\}^{2+}$ ($n=1, 2$)) is primarily responsible for the halogenation products and requires 5PhIO as a terminal oxidant. The expected small amount of initial halogenation product may be further reduced by cage escape (see above and the Supporting Information).

Halogenation due to the “resting state” (the oxido-bridged diiron(III) complex $\{[(L^n)(Cl)Fe^{III}]_2O\}^{2+}$ ($n=1, 2$)) is further supported by experiments with the dinucleating bispidine L^3 which, under the conditions described here, in a very fast reaction selectively forms the oxido-bridged diiron(III) complex

Table 2. Yield of products obtained in the reaction of $[(L^1)(Cl)Fe^{IV}=O]^+$, $[(L^2)(Cl)Fe^{IV}=O]^+$ and $\{[(L^3)(Cl)Fe^{III}]_2O\}^{2+}$ under standard conditions, where not indicated otherwise (1 equiv., 7 mM) with 5PhIO (10 equiv.) and cyclohexane (100 equiv.) in MeCN after stirring for 24 h under Ar at ambient temperature. Percentages are based on the amount of Fe^{II} complex used.

| Complex | Salt (conc. in MeCN) | $C_6H_{11}Cl$ [%] |
|-----------------------------------|----------------------|--------------------------------|
| $[(L^1)(Cl)Fe^{IV}=O]^+$ | – | 47.0 ± 4.3 ^[23] |
| $[(L^1)(Cl)Fe^{IV}=O]^+$ | NBu_4PF_6 (700 mM) | 50.4 ± 3.6 |
| $[(L^1)(Cl)Fe^{IV}=O]^+$ | NBu_4Cl (700 mM) | 14.4 ± 2.1 |
| $[(L^1)(Cl)Fe^{IV}=O]^+$ | NBu_4Cl (70 mM) | 29.6 |
| $[(L^1)(Cl)Fe^{IV}=O]^+$ | – | 0.8 ± 0.2 ^[a] |
| $[(L^1)(Cl)Fe^{IV}=O]^+$ | NBu_4Cl (100 mM) | 1.1 ± 0.1 ^[a] |
| $[(L^1)(Cl)Fe^{IV}=O]^+$ | NBu_4PF_6 (100 mM) | 1.2 ± 0.2 ^[a] |
| $[(L^2)(Cl)Fe^{IV}=O]^+$ | – | 73.6 ± 3.2 |
| $\{[(L^3)(Cl)Fe^{III}]_2O\}^{2+}$ | – | 39.8 |

[a] With 1 instead of 10 equiv. of 5PhIO , i.e., stoichiometric reaction.

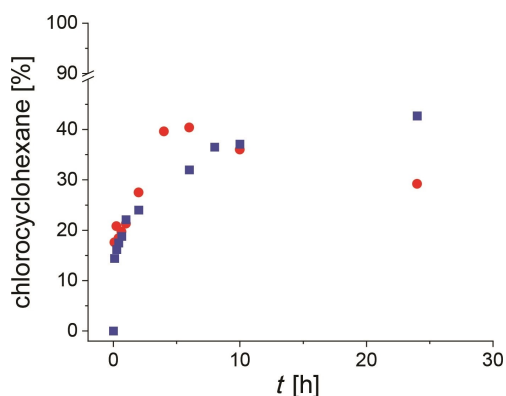


Figure 1. Comparison of the time-dependent formation of chlorocyclohexane with $[(L^1)(Cl)Fe^{IV}=O]^+$ (•) and $FeCl_2$ (•).

$\{(L^3)[(Cl)Fe^{III}]_2O\}^{2+}$.^[23] While, as expected, without added oxidant no reaction with cyclohexane occurs, addition of ³PhIO under the same conditions as for the other two bispidine-iron precursors $\{(L^3)[(Cl)Fe^{III}]_2O\}^{2+}$ produces around 40% chlorocyclohexane (Tables 2 and S13). The slightly lower yield (ca. 40 vs. 50%) might be the result of steric strain induced by the ethylene bridge and minor changes in the electronic ground state – note that the overall geometry of the oxido-bridged diiron(III) complex is enforced to *endo*-geometry with respect to the chlorido coligands, while the experimentally determined structure with L^2 has *exo*-geometry.^[23] In addition, oxidation of $\{(L^3)[(Cl)Fe^{III}]_2O\}^{2+}$ might produce a reactive intermediate leading to decay processes in addition to those observed with the L^1 and L^2 based iron oxidants. However, we consider the similar reactivities of $[(L^1)(Cl)Fe^{IV}=O]^+$, $[(L^2)(Cl)Fe^{IV}=O]^+$ and $\{(L^3)[(Cl)Fe^{III}]_2O\}^{2+}$ in the bulk reactions as a strong support for the proposed mechanistic scenario in Scheme 2, that is, selective halogenation of cyclohexane in approx. 50% yield to a large extent by oxidation with ³PhIO of the oxido-bridged diiron(III) resting state.

The two bispidine based chlorido-ferryl complexes $[(L^1)(Cl)Fe^{IV}=O]^+$ and $[(L^2)(Cl)Fe^{IV}=O]^+$ are obviously also able to halogenate substrates with lower C–H bond dissociation energies with similar yields (Table 3; BDE, cyclohexane: 99.5 kcal mol⁻¹, cyclopentane: 96.9 kcal mol⁻¹, adamantane: 98.5 kcal mol⁻¹, 96.0 kcal mol⁻¹; note that due to restricted solubility, with adamantane the reaction conditions were slightly different, and the formation of minor amounts of alcohol product are also observed).^[43,44] Importantly, with adamantane the normalized ratio of substitution at the tertiary (4 H atoms) and secondary carbons (12 H atoms, 3°/2°) can be used to distinguish between radical-based reactions and processes, where the C–H abstraction by a metal-oxido species is rate determining, and the 3°/2° ratios in radical reactions are very low (generally around 1–5), and values > 10 are associated with rate-determining C–H abstraction by a metal-oxido species and a significant life time of the substrate radical.^[13,40,45] The 3°/2° ratios of the two bispidine complexes (12.8, 13.8) are in the range of other ferryl oxidants, and this further supports the mechanism proposed in Scheme 2, that is, the bulk halogenation is as the low temperature reaction due to a high-valent iron-oxido-chlorido species.

As noted above, the very rigid bispidine cavity is too large for $Fe^{IV}=O$, and the thermodynamic instability is responsible for the exceedingly high redox potentials but might also lead to other decay pathways, that is, to decomplexation. It was

therefore of importance to also test the reactivity of free Fe^{II} and Fe^{III} ions. Indeed, with simple iron salts there is also formation of halogenated products under the condition of the reactions discussed here. The 3°/2° ratios with adamantane (8.4 and 6.5 with Fe^{II} and Fe^{III} , respectively) indicate that these halogenations are radical-based processes. Moreover, while the bispidine complexes selectively form monohalogenated products, with uncomplexed iron ions, chloride and cyclohexane as substrate significant amounts of the three possible stereoisomers of dichlorocyclohexane were also detected (see the Supporting Information). The time-dependent chlorocyclohexane formation with $FeCl_2$ as catalyst shows an increase with a maximum reached after 5 h (see Figure 1, red symbols). The subsequent decrease of the monochlorinated species due to further oxidation to dichlorinated products supports the mechanistic difference between the halogenation with the bispidine complexes and uncomplexed iron chloride. Together with the low 3/2° ratios typical for a radical-based process, this illustrates that different reaction mechanisms are in operation. Therefore, halogenation by the bispidine complexes through decomplexation and subsequent radical reaction is excluded. More importantly, the results with simple iron salts support the interpretation that $[(L^1)(Cl)Fe^{IV}=O]^+$ and $[(L^2)(Cl)Fe^{IV}=O]^+$ (and the corresponding oxido-bridged diiron(III) resting states) oxidize the organic substrates through C–H abstraction followed by a rebound step to a Cl^- coordinated to an iron-based intermediate.

Computational analysis

To further analyze the halogenation of cyclohexane by $[(L^1)(Cl)Fe^{IV}=O]^+$ and other halogenase model systems and to understand their halogenation/hydroxylation selectivity, the electronic properties of $[(L^1)(Cl)Fe^{IV}=O]^+$ and the other relevant systems (ligands L^4 , L^5 , L^6) were analyzed by density functional theory (DFT). The $Fe^{IV}=O$ center can either be high-spin (hs, $S=2$), intermediate-spin (is, $S=1$) or low-spin (ls, $S=0$), denoted as $^5FeO_{hs}$, $^3FeO_{is}$, $^1FeO_{ls}$, respectively. Among the three possible computed states, for $[(L^1)(Cl)Fe^{IV}=O]^+$ (O *trans* to N3), $^5FeO_{hs}$ is found to be the ground state, followed by $^3FeO_{is}$ at 11.9 kJ mol⁻¹ (see the Supporting Information for details). Clearly, this is not in agreement with the experiment, and problems with DFT correctly describing metal-ligand bonds in coordination compounds in general and specifically with $Fe^{IV}=O$, and the ensuing problems to accurately calculate spin state energies are well-

Table 3. Comparison of the percentage yields of the products obtained in the reaction of $[(L^1)(Cl)Fe^{IV}=O]^+$, $[(L^2)(Cl)Fe^{IV}=O]^+$, $FeCl_2$ and $FeCl_3$ (1 equiv. each) with ³PhIO (10 equiv.) and cyclopentane, cyclohexane (100 equiv.) or adamantane (10 equiv.) in abs. MeCN after stirring for 24 h at ambient temperature. The percentage yields refer to the amount of iron(II) complex used.

| Substrate | Products | $[(L^1)(Cl)Fe^{IV}=O]^+$ | $[(L^2)(Cl)Fe^{IV}=O]^+$ | $FeCl_2$ | $FeCl_3$ |
|--------------|--------------------|--------------------------|--------------------------|------------|------------|
| cyclohexane | chlorocyclohexane | 47.0 ± 4.3 | 73.6 ± 3.2 | 33.7 ± 3.5 | 39.5 ± 7.0 |
| cyclopentane | chlorocyclopentane | 40.1 ± 7.3 | 73.7 ± 5.9 | 25.3 ± 6.3 | 41.8 ± 0.3 |
| adamantane | 1-chloroadamantane | 23.6 ± 1.4 | 66.9 ± 4.7 | 28.9 ± 1.9 | 21.5 ± 2.9 |
| | 2-chloroadamantane | 5.9 ± 0.3 | 17.5 ± 0.8 | 10.6 ± 0.9 | 10.0 ± 1.3 |
| | adamantane-1-ol | 4.2 ± 0.6 | 0 | 0.8 ± 0.1 | 0 |
| | adamantane-2-ol | 0.6 ± 0.1 | 1.9 ± 0.4 | 0 | 0 |

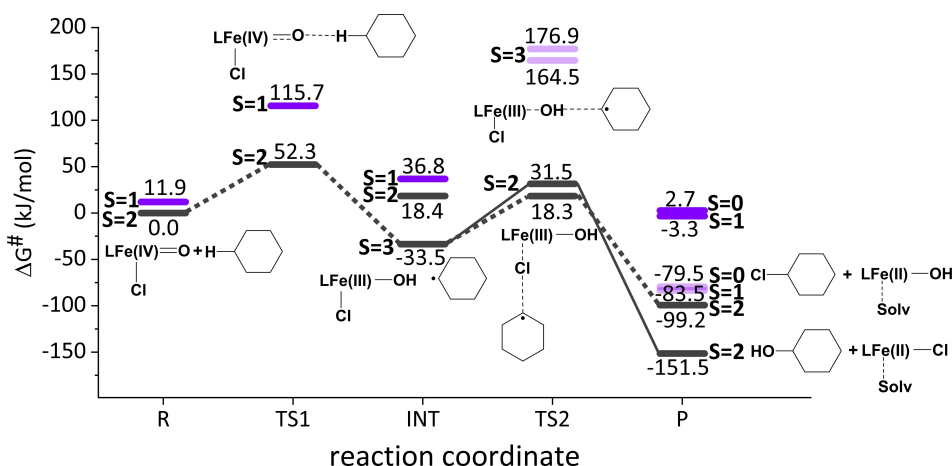


Figure 2. Computed profile for the reaction of $[(L^1)(Cl)Fe^{IV}=O]^+$ (O trans N3) with cyclohexane at the UB3LYP/def2TZVP level (PCM/MeCN).

known.^[24,26,46–48] With the setup used here (see the Experimental Section)^[49] not only for $[(L^1)(Cl)Fe^{IV}=O]^+$ but also for the other halogenase models with an established $S=1$ ground state, $[(L^5)(Cl)Fe^{IV}=O]^+$ and $[(L^6)(Cl)Fe^{IV}=O]^+$, the relative spin state energies are not correctly predicted, and only for the high-spin complex $[(L^4)(Cl)Fe^{IV}=O]^+$ the correct ground state is obtained. However, with one exception,^[50] C–H abstraction of $Fe^{IV}=O$ generally proceeds on the σ channel of the quintet surface (see above), and the accuracy of these energy barriers – specifically when only the relative barrier heights of four structurally similar systems are considered – is assumed to be acceptable.

Shown in Figure 2 is the entire computed profile for the stable isomer of $[(L^1)(Cl)Fe^{IV}=O]^+$ (O *trans* to N3) and cyclohexane, with the reactant R (the ferryl complex), the rebound intermediate INT (the Fe^{III} hydroxide-chlorido complex with the organic radical) and the product P (the Fe^{II} precursor with the two possible organic products due to halogenation or hydroxylation); a comparison with the analogous plot for the isomer with O *trans* to N7 appears in the Supporting Information, Figures S8–S10). Shown in Figure 3 are the profiles for C–H abstraction from cyclohexane of the four halogenase model systems $[(L^1)(Cl)Fe^{IV}=O]^+$, $[(L^4)(Cl)Fe^{IV}=O]^+$, $[(L^5)(Cl)Fe^{IV}=O]^+$ and $[(L^6)(Cl)Fe^{IV}=O]^+$ on the quintet surface, where all energies have been normalized to the ferryl reactant (see the Supporting Information for details). The important observation is that the barriers for C–H abstraction follow qualitatively the order of the observed rate constants, that is, with a computed barrier of 52.3 kJ mol^{-1} , the observed second-order rate with $[(L^1)(Cl)Fe^{IV}=O]^+$ is $7.6 \times 10^2 \text{ M}^{-1} \text{ s}^{-1}$ at -90°C (Table S1),^[23] the corresponding barrier and rate for $[(L^4)(Cl)Fe^{IV}=O]^+$ are 58 kJ mol^{-1} and $5 \times 10^{-2} \text{ M}^{-1} \text{ s}^{-1}$ (-40°C , toluene as substrate), and for $[(L^5)(Cl)Fe^{IV}=O]^+$ and $[(L^6)(Cl)Fe^{IV}=O]^+$ the computed barriers are much higher with 72 and $117.7 \text{ kJ mol}^{-1}$, and kinetic parameters of both are not available – the former is known to produce chlorocyclohexane,^[16] the latter does not.^[51] Therefore, the record reactivity of $[(L^1)(Cl)Fe^{IV}=O]^+$ and the relative order of

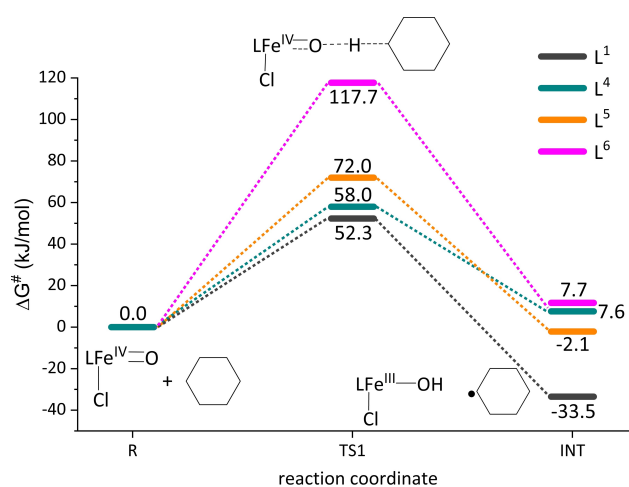


Figure 3. Computed reaction profile (UB3LYP/def2TZVP level; PCM/MeCN) for the abstraction of C–H from cyclohexane with $[(L^1)(Cl)Fe^{IV}=O]^+$, $[(L^4)(Cl)Fe^{IV}=O]^+$, $[(L^5)(Cl)Fe^{IV}=O]^+$ and $[(L^6)(Cl)Fe^{IV}=O]^+$ on the quintet surface, where all reactant energies have been set to 0.0 kJ mol^{-1} .

activities with all four oxidants are reproduced, although not quantitatively.

The current DFT analysis does not allow to unambiguously relate the barrier heights to specific electronic properties (see the Supporting Information for details), and in view of the limits of the DFT model this is not surprising. An important feature of the energetics shown in Figure 3 is the driving force, that is, it is by far largest (by $> 30 \text{ kJ mol}^{-1}$) for $[(L^1)(Cl)Fe^{IV}=O]^+$, and this is due to the large and rigid bispidine cavity and agrees with experimental observations and computational studies: bispidine $Fe^{IV}=O$ complexes are among the strongest ferryl oxidants known to date.^[32–35] Another feature of importance is the energy difference between the triplet and the quintet states, and this is very small for $[(L^1)(Cl)Fe^{IV}=O]^+$ and tunable with the coligand: the computed triplet-quintet gap for MeCN, Cl^- and Br^- as coligands is in good agreement with observed $d_{x^2-y^2}$ electronic transitions and with the observed reactivities (see above).^[23]

Additional experimental and computational studies will hopefully help to more thoroughly understand these various aspects and their relevance for the observed reactivity.

More important in terms of the halogenation selectivity are the energy barriers for the transformation of the $[(L^n)Fe^{III}(OH)(Cl)]^+$ /cyclohexyl radical intermediates ($n=1,4,5,6$) to the chlorocyclohexane and cyclohexanol products together with the $[(L^n)Fe^{II}(MeCN)(X)]^+$ species ($n=1,4,5,6$; $X=OH,Cl$). These barriers are depicted in Figure 4, where the energies of the iron(III)/radical intermediates for all four ligands are set to 0.0 kJ mol^{-1} , and the relative energy barriers clearly reproduce the observed trends: with an energetic preference of over 13 kJ mol^{-1} $[(L^1)(Cl)Fe^{IV}=O]^+$ leads to selective halogenation, with an energy difference of 6 kJ mol^{-1} $[(L^5)(Cl)Fe^{IV}=O]^+$ has a 85% preference for chlorocyclohexane, with a 8 kJ mol^{-1} difference in the barrier $[(L^4)(Cl)Fe^{IV}=O]^+$ produces 78% chlorocyclohexane, and $[(L^6)(Cl)Fe^{IV}=O]^+$ with an 18 kJ mol^{-1} lower barrier for hydroxylation does not form any halogenated product at all. That is, the computed relative barriers (Figure 4) are in excellent agreement with the experimental observations (Table 1). Importantly, the two barriers for $[(L^1)(Cl)Fe^{IV}=O]^+$ (51.8 and 65 kJ mol^{-1}) are both larger than 50 kJ mol^{-1} , thus implying a relatively large lifetime of the intermediate, and this is corroborated with the observed cage escape, supported by two types of experiments (see above).^[23] Interestingly, the computed lifetimes of the intermediate for the other three halogenase models are of a similar order (all $>45 \text{ kJ mol}^{-1}$), and for $[(L^4)(Cl)Fe^{IV}=O]^+$ and $[(L^5)(Cl)Fe^{IV}=O]^+$, where cage escape has also been probed, the suppression of the rebound pathway by dioxygen is of similar efficiency as for the bispidine complex discussed here.^[16] The experimental data as well as the computed life-time (energy barriers in Figure 4) indicate that cage escape is a problem, leading to a reduced yield of the low

temperature reaction but is not the major or only reason, that is, formation of the oxido-bridged diiron(III) complex (resting state) is of major importance.

A thorough analysis of the electronics of the twice four transition states of all systems discussed here, involving spin densities, charge distributions (see the Supporting Information for details) does not suggest electronic reasons for the varying halogenation selectivities. With the note of caution due to the inherent problems with DFT calculations for this sort of system (see above) we interpret this observation as mainly steric reasons to be responsible for the observed selectivities. This is supported by the experimental observation that a reduction of the steric demand of the L^1 based ferryl oxidant by removal of the N7-methyl substituent (L^2) leads to a significant increase of the chlorocyclohexane yield (74 vs. 47%); note however, that electronic effects might also be partially responsible for the significant increase in product yield, see above.

Conclusions

Although $[(L^n)(Cl)Fe^{IV}=O]^+$ ($n=1, 2$) has a triplet ground state, it is the most reactive mononuclear ferryl complex known with a reactivity similar to that of enzymes. Moreover, reaction with cyclohexane leads to selective chlorination, and the yield of chlorocyclohexane from this stoichiometric reaction can be over 70% with respect to the iron complex. The reaction is shown to proceed via initial C–H abstraction (supported among others by the observed selectivity with adamantane as substrate) and cyclohexyl radical rebound to an $[(L^n)Fe^{III}(OH)(Cl)]^+$ derived intermediate (supported by a strong suppression of the halogenation yield when free Cl^- is added, i.e., only iron-bound Cl^- leads to the halogenated product). However, the exceed-

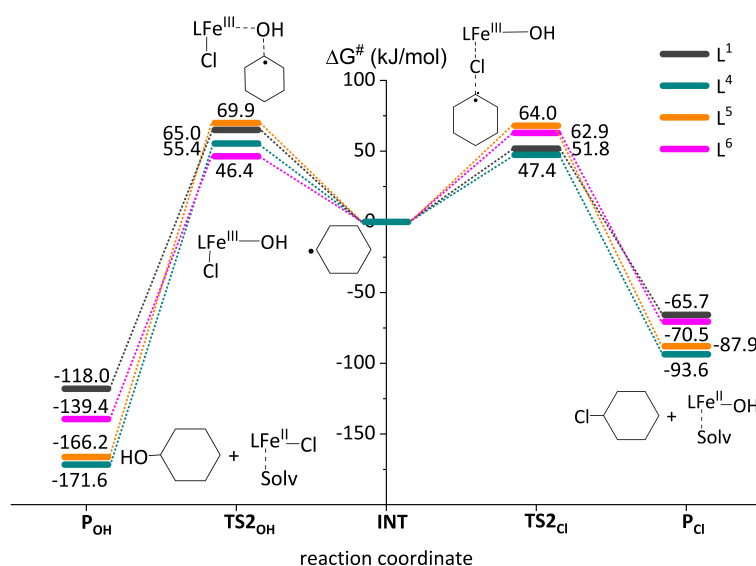


Figure 4. Computed reaction profile (UB3LYP/def2TZVP level; PCM/MeCN) for the hydroxylation (left) vs. halogenation (right) of $[(L^1)(Cl)Fe^{IV}=O]^+$, $[(L^4)(Cl)Fe^{IV}=O]^+$, $[(L^5)(Cl)Fe^{IV}=O]^+$ and $[(L^6)(Cl)Fe^{IV}=O]^+$ with cyclohexane. the rebound part of the reaction is shown, starting with the $[(L^n)Fe^{III}(OH)(Cl)]^+$ /cyclohexyl radical intermediate set to 0.0 kJ mol^{-1} . A full reaction profile for $[(L^1)(Cl)Fe^{IV}=O]^+$ is given in the Supporting Information.

ingly fast C–H abstraction is followed by a quite stable rebound intermediate that is responsible for some cage escape, as shown by quenching of the substrate radical intermediate by dioxygen or TEMPO. This is supported by DFT analysis, which indicates a relatively long lifetime of the $[(L^n)Fe^{III}(OH)(Cl)]^+$ /substrate radical rebound precursor, and this is a common observation for all halogenase models discussed here. Moreover, the oxido-bridged diiron(III) “resting state”, produced in an efficient decay channel of the $[(L^n)(Cl)Fe^{IV}=O]^+$ oxidant in the presence of excess 3PhIO is, to a large extent, responsible for product formation. Whether this reacts as a diiron(IV) oxidant or decays to a mononuclear $Fe^{IV}=O$ species needs to be further evaluated. The total yield of up to >70% chlorocyclohexane with respect to the $[(L^1)Fe^{II}(Cl)_2]$ precursor is remarkable and indicates a high stability of the $[(L^1)(Cl)Fe^{IV}=O]^+$ active oxidant.

Experimental Section

All chemicals and reagents were purchased from commercial sources (ABCR; ACROS, Sigma-Aldrich; TCI). Dry solvents were stored over molecular sieves and were used without further purification. Preparation and handling of air-sensitive materials were carried out using either Schlenk techniques or in a glovebox under argon.

Gas chromatographic separations were carried out using a Varian GC3900 with an attached CP-8410 autosampler from Agilent, on a BP10 column (30 m, 0.25 mm, 0.25 μ m layer thickness) from SGE with helium as carrier gas. The detection was carried out with a flame ionization detector (FID), the quantification was done by calibrating the possible products.

Gas chromatography coupled mass spectra (GC-MS) were measured with an Ultra Trace GC coupled to an ISQ Single Quadrupole MS from Thermo Fisher Scientific. The separation was performed using a TG-1701MS column (30 m length, 0.25 mm diameter, 0.25 μ m) from Thermo Scientific with helium as carrier gas and coupled FID. The spectra were analyzed using the ACD/Spectrum Processor 2017.2 software from ACD/Labs.

The bispidine-iron(II) complexes and soluble iodosylbenzene (3PhIO) were synthesized according to literature procedures.^[14,23,52–59] Reactions for chlorocyclohexane formation were carried out in the glovebox with iron complex concentrations of 7 mM and a total reaction volume of 2 mL (dry MeCN). To the particular iron complex, cyclohexane (100 equiv.), NBu_4X ($X=PF_6, Cl$; 700 mM, if used) and 3PhIO (10 equiv.) were added and, after stirring at room temperature for 24 h (or after the desired time for time dependent measurements), to this reaction mixture was added the internal standard naphthalene or nitrobenzene for the GC measurement (see the Supporting Information for the calibration of the GC instrument). Then, the reaction solution was filtered over a pipette column (silica) to remove the iron complex. The column was rinsed with 3 mL MeCN. All reactions were carried out at least 4 times for the determination of averages and standard derivation (note, that for the data point $[L^2FeCl_2]+$ cyclopentane, only three measurements were carried out). For experiments with adamantane and cyclopentane as substrate no inert salt was added. Because of the low solubility of adamantane in MeCN, substrate concentrations of 70 mM (10 equiv.) were used. Halogenation reactions with $FeCl_2$ and $FeCl_3$ were carried out in the glovebox with iron salt concentrations of 7 mM and a total reaction volume of 2 mL (dry MeCN). Substrate and oxidant concentrations were used as described [cyclohexane 700 mM (100 equiv.), adamantane 70 mM (10 equiv.), 3PhIO (10 equiv.)]. The reaction solutions were stirred for

24 h at RT (or for the desired time for time dependent measurements), and the workup and quantification was carried out as described above.

All DFT calculations were performed using the Gaussian 09 suite of programs.^[60] The geometries were optimized using the B3LYP functional with def2-TZVP basis set^[61–63] This functional has been employed by us and others earlier to predict the correct spin state energetic of several mononuclear metal complexes. Frequency calculation on the optimized structures was undertaken to confirm the minima on the potential-energy surface (PES) and also to obtain free energy and zero-point energy corrections. The solvation energies were computed by using polarizable continuum model (PCM) solvation model where MeCN ($\epsilon=35.688$) has been used as the solvent. All reported energies are B3LYP solvent-phase energies incorporating free energy corrections at 298.15 K, unless otherwise mentioned.

Supporting Information: Details of the halogenation experiments and GC/MS as well as GC procedures, and data of the product analyses as well as detailed computational data are given as Supporting Information.

Acknowledgements

Financial support by the Heidelberg University, by the state Baden-Württemberg (a bursary by the Landesgraduiertenförderung), by the European Cooperation in Science and Technology (COST), the German Science Foundation (DFG), and the Heidelberg Graduate School of Computational Methods for the Sciences (HGS) are gratefully acknowledged. This study was conducted within the Max Planck School Matter to Life, supported by the BMBF in collaboration with the Max Planck Society. We are grateful for computational resources provided by the bwForCluster JUSTUS, funded by the Ministry of Science, Research and Arts and the Universities of the State of Baden-Württemberg, Germany, within the framework program bwHPC–C5. Open Access funding enabled and organized by Projekt DEAL.

Conflict of Interest

The authors declare no conflict of interest.

Keywords: biomimetic coordination chemistry · C–H activation · DFT calculations · non-heme-iron · reaction mechanism

- [1] *Modern Oxidation Methods* (Ed.: J.-E. Bäckvall), Wiley-VCH, Weinheim, 2004.
- [2] F. Cavani, J. H. Teles, *ChemSusChem* 2009, 2, 508–534.
- [3] A. Podgorssek, M. Zupan, J. Iskra, *Angew. Chem. Int. Ed.* 2009, 48, 8424–8450; *Angew. Chem.* 2009, 121, 8576–8603.
- [4] S. Hong, Y.-M. Lee, K. Ray, W. Nam, *Coord. Chem. Rev.* 2017, 334, 25–42.
- [5] L. Vicens, G. Olivo, M. Costas, *ACS Catal.* 2020, 10, 8611–8631.
- [6] U. Dutta, S. Maiti, T. Bhattacharya, D. Maiti, *Science* 2021, 372, 701.
- [7] S. Rana, J. P. Biswas, S. Paul, A. Paik, D. Maiti, *Chem. Soc. Rev.* 2021, 50, 243–472.
- [8] F. H. Vaillancourt, E. Yeh, D. A. Vosburg, S. Garneau-Tsodikova, C. T. Walsh, *Chem. Rev.* 2006, 106, 3364–3378.

- [9] C. Krebs, D. Galonici Fujimori, C. T. Walsh, J. M. Bollinger Jr., *Acc. Chem. Res.* **2007**, *40*, 484–492.
- [10] M. L. Matthews, C. S. Neumann, L. A. Miles, T. L. Grove, S. J. Booker, C. Krebs, C. T. Walsh, J. M. Bollinger Jr., *Proc. Natl. Acad. Sci. USA* **2009**, *106*, 17723–17728.
- [11] S. D. Wong, M. Srncic, M. L. Matthews, L. V. Liu, Y. Kwak, K. Park, C. B. Bell, E. E. Alp, J. Zhao, Y. Yoda, S. Kitao, M. Seto, C. Krebs, J. M. Bollinger, E. I. Solomon, *Nature* **2013**, *499*, 320–323.
- [12] M. Srncic, J. E. I. Solomon, *J. Am. Chem. Soc.* **2017**, *139*, 2396–2407.
- [13] T. Kojima, R. A. Leising, S. Yan, L. Que Jr., *J. Am. Chem. Soc.* **1993**, *115*, 11328–11335.
- [14] P. Comba, S. Wunderlich, *Chem. Eur. J.* **2010**, *16*, 7293–7299.
- [15] O. Planas, M. Clémancey, J. M. Latour, A. Company, M. Costas, *Chem. Commun.* **2014**, *50*, 10887–10890.
- [16] M. Puri, A. N. Biswas, R. Fan, Y. Guo, L. Que, *J. Am. Chem. Soc.* **2016**, *138*, 2484–2487.
- [17] N. Kannan, A. Patil, A. Sinha, *Dalton Trans.* **2020**, *49*, 14344–14360.
- [18] J. P. Biswas, S. Guin, D. Maiti, *Coord. Chem. Rev.* **2020**, *408*, 213174.
- [19] A. Thibon, J. England, M. Martinho, V. G. Young Jr., J. R. Frisch, R. Guillot, J.-J. Girerd, E. Münck, L. Que Jr., F. Banse, *Angew. Chem. Int. Ed.* **2008**, *47*, 7064–7067; *Angew. Chem.* **2008**, *120*, 7172–7175.
- [20] S. Chatterjee, T. K. Paine, *Angew. Chem. Int. Ed.* **2016**, *55*, 7717–7722; *Angew. Chem.* **2016**, *128*, 7848–7853.
- [21] R. Jana, D. Sheet, S. Chatterjee, T. Paine, *Inorg. Chem.* **2018**, *57*, 8769–8777.
- [22] S. Rana, J. P. Biswas, A. Sen, M. Clémancey, G. Blondin, J.-M. Latour, G. Rajaraman, D. Maiti, *Chem. Sci.* **2018**, *9*, 7843–7858.
- [23] M. Abu-Odeh, K. Bleher, N. J. Britto, P. Comba, M. Gast, M. Jaccob, M. Kerscher, S. Krieg, M. Kurth, *Chem. Eur. J.* **2021**, *27*, 11377–11390.
- [24] P. Comba, D. Faltermeier, S. Krieg, B. Martin, G. Rajaraman, *Dalton* **2020**, *49*, 2888–2894.
- [25] S. Ye, F. Neese, *Curr. Opin. Chem. Biol.* **2009**, *12*, 89–98.
- [26] C. Geng, S. Ye, F. Neese, *Angew. Chem. Int. Ed.* **2010**, *49*, 5717–5720.
- [27] L. Roy, *ChemPlusChem* **2019**, *84*, 893–906.
- [28] D. Mandal, D. Mallick, S. Shaik, *Acc. Chem. Res.* **2018**, *51*, 107–117.
- [29] C. Bleiholder, H. Börzel, P. Comba, R. Ferrari, A. Heydt, M. Kerscher, S. Kuwata, G. Laurency, G. A. Lawrence, A. Lienke, B. Martin, M. Merz, B. Nuber, H. Pritzkow, *Inorg. Chem.* **2005**, *44*, 8145–8155.
- [30] P. Comba, A. Lienke, *Inorg. Chem.* **2001**, *40*, 5206–5209.
- [31] A. Anastasi, P. Comba, J. McGrady, A. Lienke, H. Rohwer, *Inorg. Chem.* **2007**, *46*, 6420–6426.
- [32] P. Comba, S. Fukuzumi, H. Kotani, S. Wunderlich, *Angew. Chem. Int. Ed.* **2010**, *49*, 2622–2625; *Angew. Chem.* **2010**, *122*, 2679–2682.
- [33] D. Wang, K. Ray, M. J. Collins, E. R. Farquhar, J. R. Frisch, L. Gomez, T. A. Jackson, M. Kerscher, A. Waleska, P. Comba, M. Costas, E. Münck, L. Que Jr., *Chem. Sci.* **2013**, *4*, 282–291.
- [34] P. Comba, S. Fukuzumi, C. Koke, A. M. Löhr, J. Straub, *Angew. Chem. Int. Ed.* **2016**, *55*, 11129–11133; *Angew. Chem.* **2016**, *128*, 11295–11299.
- [35] P. Comba, D. Faltermeier, B. Martin, *Z. Anorg. Allg. Chem.* **2020**, *646*, 1839–1845 (Special Issue for H. W. Roesky).
- [36] Note that in addition to electronic effects of the substituent on the ligand field strength of the amine, steric effects might also be of importance.^[37]
- [37] A. Bentz, P. Comba, R. J. Deeth, M. Kerscher, H. Pritzkow, B. Seibold, H. Wadepohl, *Inorg. Chem.* **2008**, *47*, 9518.
- [38] P. Comba, M. Morgen, H. Wadepohl, *Inorg. Chem.* **2013**, *52*, 6481–6501.
- [39] P. Comba, M. Maurer, P. Vadivelu, *J. Phys. Chem. A* **2008**, *112*, 13028–13036.
- [40] P. Comba, M. Maurer, P. Vadivelu, *Inorg. Chem.* **2009**, *48*, 10389–10396.
- [41] Further experimental support for the mechanism in Scheme 2 is presented in the current publication. However, as general in mechanistic work, admittedly, there are additional possible experiments that may (or may not) support our current interpretation, and some are currently in progress.
- [42] So far only for the self-decay, i.e., formation of the oxido-bridged diiron(III) complex a preliminary kinetic analysis was performed (pathway with k_2 in Scheme 2). Note also that, while for $[(L^1)(Cl)Fe^{IV}=O]^+$ the position of the oxido group trans to N3 has been verified experimentally,^[21] for $[(L^2)(Cl)Fe^{IV}=O]^+$ this only is an assumption, and a differing geometry could also explain the difference in the ligand field.)
- [43] G. H. Kruppa, J. L. Beauchamp, *J. Am. Chem. Soc.* **1986**, *108*, 2162–2169.
- [44] Z. Tian, A. Fattahi, L. Lis, S. R. Kass, *J. Am. Chem. Soc.* **2006**, *128*, 17087–17092.
- [45] M. Costas, K. Chen, L. Que Jr, *Coord. Chem. Rev.* **2000**, *200*, 517–544.
- [46] M. Atanasov, P. Comba, B. Martin, V. Müller, G. Rajaraman, H. Rohwer, S. Wunderlich, *J. Comput. Chem.* **2006**, *27*, 1263–1277.
- [47] S. P. De Visser, M. G. Quesne, B. Martin, P. Comba, U. Ryde, *Chem. Commun.* **2014**, *50*, 262–282. (Special web themed issue “Biological Oxidation Reactions”).
- [48] P. Verma, Z. Varga, J. E. M. N. Klein, C. J. Cramer, L. Que Jr, D. G. Truhlar, *Phys. Chem. Chem. Phys.* **2017**, *19*, 13049–13069.
- [49] The DFT setup used here might not be the optimum for spin state energies of ferryl complexes but is often used in this context.
- [50] C. Kupper, B. Mondal, J. Serrano-Plana, I. Klawitter, F. Neese, M. Costas, S. Ye, F. Meyer, *J. Am. Chem. Soc.* **2017**, *139*, 8939–8949.
- [51] Note that the computed barriers as well as the observed rates have to be inferred with caution: i) the second-order rate of $[(L^1)(Cl)Fe^{IV}=O]^+$ has so far only been deduced from three concentrations, and the published kinetic data of the other complexes refer to different conditions; ii) the computed spin ground state of the reactant is wrong for three of the complexes, and this type of DFT energy has error limits of at least 10 kJmol⁻¹.
- [52] H. Börzel, P. Comba, H. Pritzkow, *J. Chem. Soc. Chem. Commun.* **2001**, 97–98.
- [53] H. Börzel, P. Comba, K. S. Hagen, M. Merz, Y. D. Lampeka, A. Lienke, G. Linti, H. Pritzkow, L. V. Tsybal, *Inorg. Chim. Acta* **2002**, *337*, 407–419.
- [54] B. V. Mephrathu, J. D. Protasiewicz, *Arkivoc* **2003**, 83–90.
- [55] S. E. Gibson, N. Guillo, A. J. P. White, D. J. Williams, *J. Chem. Soc.-Perkin Trans.* **1996**, *1*, 2575–2581.
- [56] D. Macikenas, E. Skrzypczak-Jankun, J. D. Protasiewicz, *J. Am. Chem. Soc.* **1999**, *121*, 7164–7165.
- [57] P. Comba, L. Grimm, C. Orvig, K. Rück, H. Wadepohl, *Inorg. Chem.* **2016**, *55*, 12531–12543.
- [58] U. Kuhl, W. Englberger, M. Haurand, U. Holzgrabe, *Arch. Pharm. Pharm. Med. Chem.* **2000**, *333*, 226–230.
- [59] P. Comba, H. Rudolf, H. Wadepohl, *Dalton Trans.* **2015**, *44*, 2724–2736.
- [60] M. J. Frisch, G. W. Trucks, H. B. Schlegel, G. E. Scuseria, M. A. Robb, J. R. Cheeseman, G. Scalmani, V. Barone, B. Mennucci, G. A. Petersson, H. Nakatsuji, M. Caricato, X. Li, H. P. Hratchian, A. F. Izmaylov, J. Bloino, G. Zheng, J. L. Sonnenberg, M. Hada, M. Ehara, K. Toyota, R. Fukuda, J. Hasegawa, M. Ishida, T. Nakajima, Y. Honda, O. Kitao, H. Nakai, T. Vreven, J. A. Montgomery Jr., J. E. Peralta, F. Ogliaro, M. Bearpark, J. J. Heyd, E. Brothers, K. N. Kudin, V. N. Staroverov, T. Keith, R. Kobayashi, J. Normand, K. Raghavachari, A. Rendell, J. C. Burant, S. Iyengar, J. Tomasi, M. Cossi, N. Rega, N. J. Millam, M. Klene, J. E. Knox, J. B. Cross, V. Bakken, C. Adamo, J. Jaramillo, R. Gomperts, R. E. Stratmann, O. Yazyev, A. J. Austin, R. Cammi, C. Pomelli, J. W. Ochterski, R. L. Martin, K. Morokuma, V. G. Zakrzewski, G. A. Voth, P. Salvador, J. J. Dannenberg, S. Dapprich, A. D. Daniels, O. Farkas, J. B. Foresman, J. V. Ortiz, J. Cioslowski, D. J. Fox, *Gaussian09, revision A.02*, Gaussian, Inc., Wallingford CT, **2013**.
- [61] A. D. Becke, *Phys. Rev. A* **1988**, *38*, 3098–3100.
- [62] J. P. Perdew, *Phys. Rev. B* **1986**, *33*, 8822–8824.
- [63] J. Zheng, X. Xu, D. G. Truhlar, *Theor. Chem. Acc.* **2011**, *128*, 295–305.

Manuscript received: September 22, 2021
Accepted manuscript online: November 18, 2021
Version of record online: December 7, 2021